

A two-lobe Journal Bearing with adjustable Gap Geometry for Vibration Reduction of flexible Rotors

B. Pfau, R. Markert

Flexible rotors in journal bearings can exhibit large vibration amplitudes during the passage of bending critical speeds. To reduce these vibrations, a two-lobe journal bearing with adjustable gap geometry is presented. By an adjustment of the gap height, stiffness and damping properties of the bearing and as a consequence the damping ratio of the rotor system can be varied during the operation. When the system passes a critical speed in a run-up process, a large gap is adjusted for higher damping. After the resonance pass through, the gap height is reduced to increase the load carrying capacity and to enlarge the stability margin. Investigating the Jeffcott rotor in adjustable journal bearings demonstrates the basic effects. For a validation, a test rig is set up and a related mathematical model is created. Various experiments are made and compared with numerical results.

1 Introduction

Journal bearings exist in different geometric designs. At this, the classical cylindrical bearing has the simplest geometry with respect to calculation and manufacturing. A disadvantage is a high susceptibility to self-excited vibrations. Hence, multi-lobe bearings having better stability properties are used for applications with low Sommerfeld numbers¹, e. g. due to high rotational speeds. Depending on the designing with respect to resonance behavior, onset speed of instability and load carrying capacity, large vibrations amplitudes may occur passing bend-critical speeds. To reduce these vibrations, a journal bearing with adjustable gap geometry is presented.

In recent years, different types of active and controllable journal bearings were developed and are increasingly found in the literature. The current state of research on controllable oil film bearings can be found in an overview article from Santos (2011). Many of the existing concepts incorporate movable (Ulbrich and Althaus (1989); Althaus (1991); Wu and de Queiroz (2010)) or flexible bearing pads (Krodkiwski et al. (1997)). Other concepts apply external forces on the bearing shell or on the journal, for example magnetically (El-Shafei and Dimitri (2010); Fürst and Ulbrich (1988)) or piezo-mechanically (Przybylowicz (2004); Tuma et al. (2013)), without changing the bearing's gap geometry. Furthermore there are also bearings that utilize an active oil injection as suggested from Santos and Scalabrin (2003) and Santos (2011). An unconventional bearing is shown by Martin and Parkins (2002), here the outer part is rotating and the inlying stator is able to vary the gap geometry by use of adjustable pins. In most of the cases, a PID controller is used.

The concept of a journal bearing with variable gap geometry for vibration reduction during the resonance pass trough was firstly presented in a previous project. The results are to find in papers of Chasalevris and Dohnal (2012, 2014, 2015). In this paper a new design is introduced, which differs significantly from the first version, since the adjustment mechanism is installed in the upper part of the bearing. This has the advantage, that the mechanism is not loaded by the self-weight of the rotor. Figure 1 shows the working principle of the adjustable bearing, which is basically a lemon bore bearing in horizontal construction design. The lower segment is fixed, the upper one can be moved along the vertical direction. The movement, which is in the shown investigations constant for certain values, leads to a change of the fluid film thickness h as well as to a change of the geometric shape. The related mathematical quantity is called preload factor δ , a measure for the geometric deviation of the lemon bore shape ($0 < \delta < 1$) in comparison to the cylindrical shape ($\delta = 0$). The basic idea of an adjustable lemon bore bearing was for the first time presented by Pfau et al. (2015) and somewhat later by Becker and Seemann (2015), whereby both publications deal with a time-periodic preload factor to increase the stability limit. This topic is also investigated by Breunung et al. (2017). A constructional realization of the bearing is shown in detail by Pfau and Markert (2016).

¹ $S_o = F_{stat} \psi^2 / (B D \eta_{oil} \Omega)$

Due to an adjustment of the gap geometry, stiffness and damping properties of the bearing are varied during the operation in dependence of the rotational speed. When the system passes a bend-critical speed in a run up process, a low preload factor (larger gap) is adjusted for higher damping. Since this setup is susceptible to stability problems and the load carrying capacity is comparatively low, the preload factor is increased after passing the resonance.

2 Description and Modeling of the Journal Bearing

At first, figure 1 is explained in detail. The journal rotates with an angular velocity Ω , the deflection is described by the eccentricity e and the angle ϑ (respectively w_L in z -direction and v_L in y -direction). The radius of the journal is given by R_Z . The segments of the sliding surfaces are all having the same radius of R_S . Thus, the gap function of the i -th ($i=1, 2$) segment is expressed by

$$h_i = (R_S - R_Z) - e \cos(\vartheta - \gamma) + h_{p,i} \cos(\vartheta - \psi_i). \quad (1)$$

At this, the latter term describes an offset between the centre of the i -th segment and the origin of ordinates (see also Pfau et al. (2015)). In the following, the term $(R_S - R_Z) = h_n$ is denoted as *nominal clearance*. It is appropriate to use it as reference quantity, due to the fact that it is constant and independent of the segment's movement. Since the lower segment is fixed ($h_{p,1} = 0$), the preload factor can be calculated to

$$\delta = h_{p,2} / (2h_n). \quad (2)$$

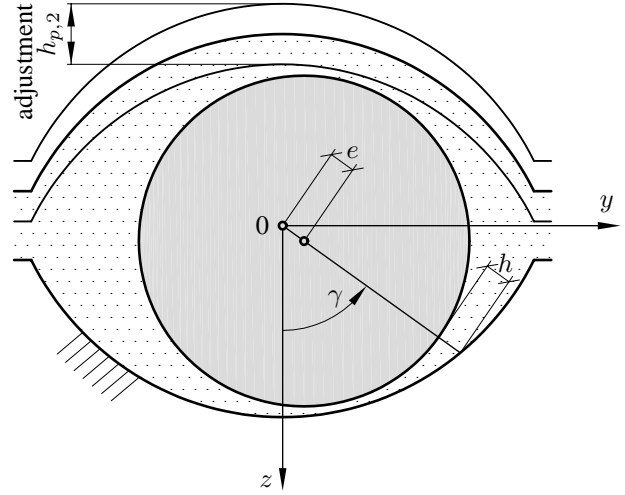


Figure 1. Lemon bore bearing in horizontal construction design; adjustment of the upper segment

The calculation of the bearing forces is performed separated for the individual segments by numerical integration of the Reynolds differential equation of lubricating film theory, see e. g. Lang and Steinhilper (1978),

$$\frac{1}{R_S^2} \frac{\partial}{\partial \vartheta} \left(h^3 \frac{\partial p}{\partial \vartheta} \right) + \frac{\partial}{\partial x} \left(h^3 \frac{\partial p}{\partial x} \right) = 6\eta_{oil} \left(\Omega \frac{\partial h}{\partial \vartheta} + 2 \frac{\partial h}{\partial t} \right), \quad (3)$$

which describes the pressure distribution $p(\vartheta, x)$ in dependence of the segment radius R_S , the gap function h , the angular velocity Ω and the oil viscosity η_{oil} . Integrating the pressure distribution yields the forces acting on the journal, F_z and F_y . The solution procedure is based on a finite volume method (see Pfau (2012) or Köhl (2015) for details). The bearing model is verified by experimentally determined data from Glienicke (1966) and numerically determined data from Someya (1989).

The fluid-film forces depend on vertical and horizontal position (w_L and v_L) and the corresponding velocities of the journal, which is in general expressed by a nonlinear relationship, $F_{z,y} = F_{z,y}(w, v, \dot{w}, \dot{v}) = F_{z,y}(e, \vartheta, \dot{e}, \dot{\vartheta})$. If the journal performs small vibrations around an equilibrium position $(w_{L,0} | v_{L,0})$, the fluid film force can be linearized which yields

$$\begin{bmatrix} \Delta F_z \\ \Delta F_y \end{bmatrix} = \begin{bmatrix} b_{zz} & b_{zy} \\ b_{yz} & b_{yy} \end{bmatrix} \begin{bmatrix} \Delta \dot{w}_L \\ \Delta \dot{v}_L \end{bmatrix} + \begin{bmatrix} k_{zz} & k_{zy} \\ k_{yz} & k_{yy} \end{bmatrix} \begin{bmatrix} \Delta w_L \\ \Delta v_L \end{bmatrix}. \quad (4)$$

Equation (4) contains the stiffness coefficients k_{ij} as well as the damping coefficients b_{ij} . Both depend on the Sommerfeld number as well as on the preload factor. For simplicity, the letter Δ is neglected hereinafter.

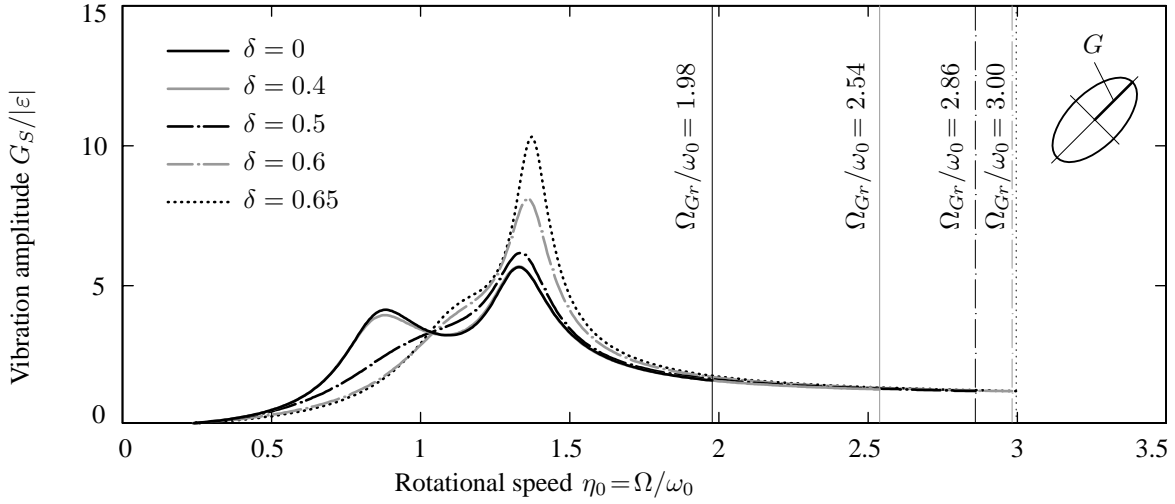


Figure 2. Vibration amplitude of the disc $G_S/|\varepsilon|$ and onset speed of instability for different preload factors δ (parameters: $S_{O0} = 1$, $\kappa = 0.5$, $\mu = 0$, $B/D = 0.5$)

3.1 Reduction of the Amplitudes during Resonance pass trough

Figure 3 shows the maximum amplitudes of $G_S/|\varepsilon|$ in dependence of the specific Sommerfeld number S_{O0} for a constant value of $\kappa = 1$. It can be seen, that especially for low Sommerfeld numbers the maximum amplitudes differ significantly. Concerning to the amplitude reduction, this is the application area of the adjustable journal bearing. For high Sommerfeld numbers the effect vanishes. This is because the journal center is located at low position on the locus (Gümbel curve) and the pressure build-up occurs mainly in the lower segment.

To evaluate the potential for vibration suppression, the maximum amplitudes are compared to a lemon bore bearing with a typical preload factor of $\delta = 0.65$ (see also DIN (1996) or Glienicke (1966)). As a measure, the quantity

$$R = 1 - \frac{G_{max,\delta_i}}{G_{max,\delta=0.65}} \quad \text{with} \quad \delta_i = 0, 0.4, 0.5 \text{ and } 0.6 \quad (6)$$

is defined. Figure 4 shows R for different values of κ . As already mentioned, a vibration suppression can only be achieved for small specific Sommerfeld numbers. Beyond this, the parameter κ plays an important role. For small values of κ , the gradient of R with respect to S_{O0} is relatively weak in comparison to bigger values of κ , which results in a larger application area. If κ is getting larger, in other words the shaft stiffness decreases in comparison

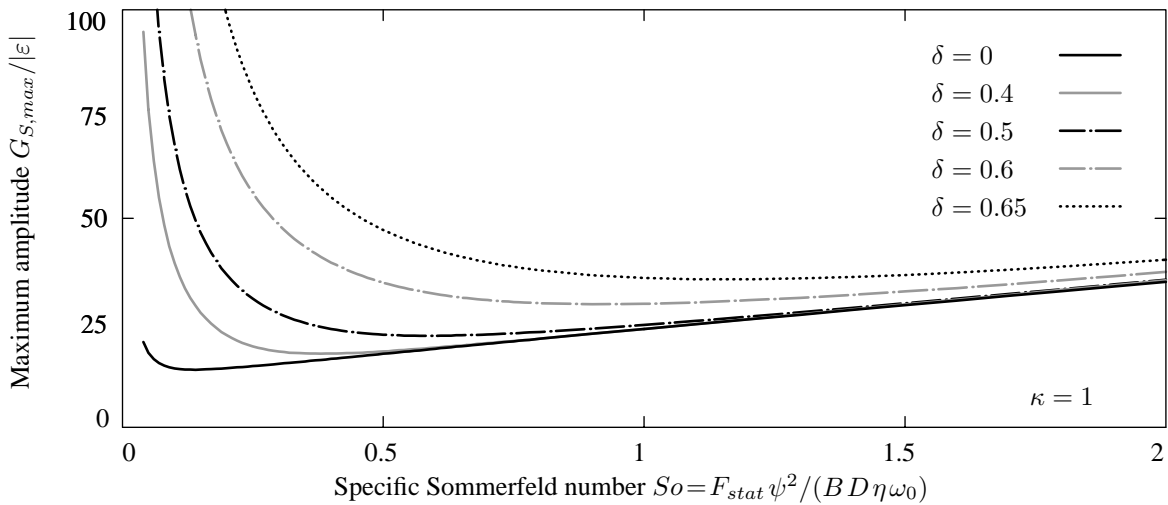


Figure 3. Maximum amplitudes $G_{S,max}/|\varepsilon|$ in dependence of the specific Sommerfeld number S_{O0} for different preload factors δ (parameters: $S_{O0} = 1$, $\kappa = 1$, $\mu = 0$, $B/D = 0.5$)

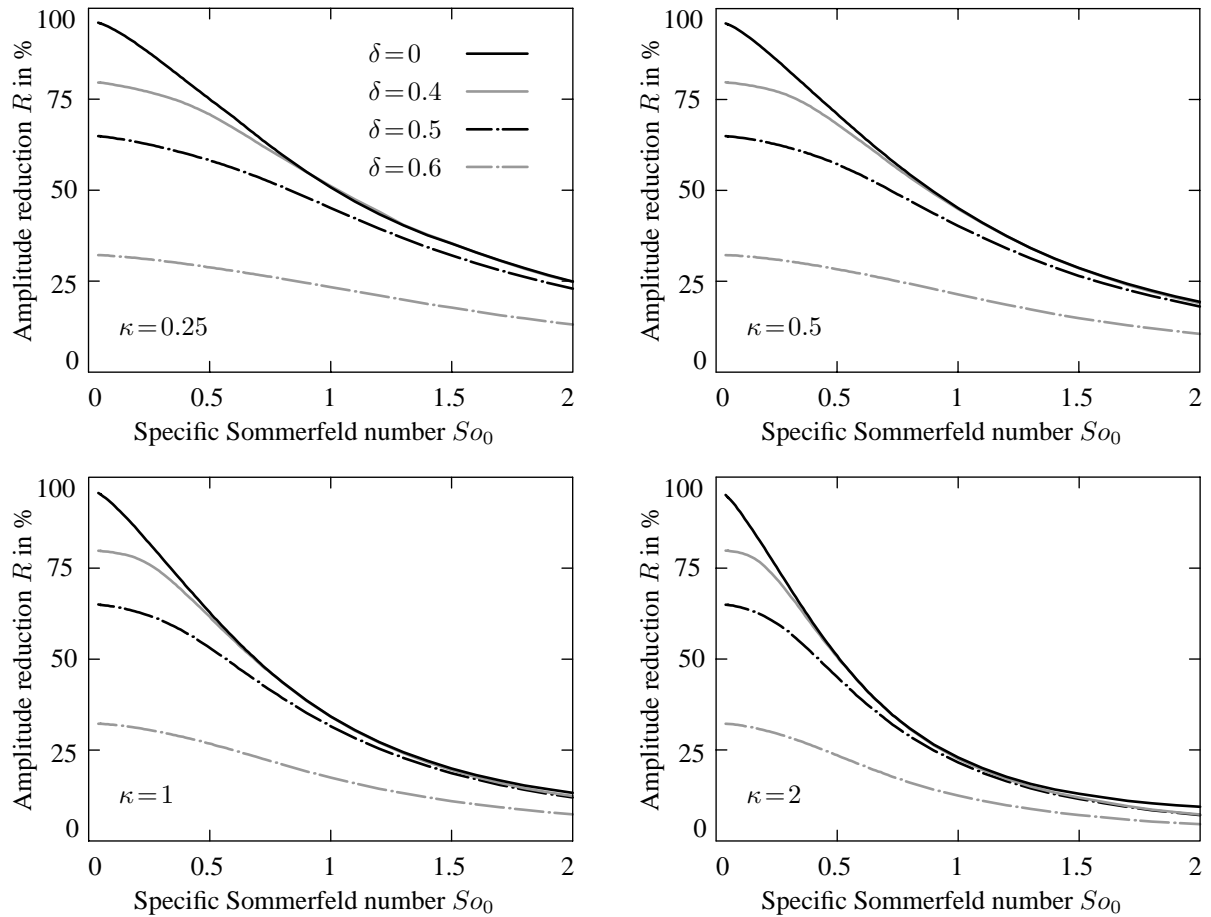


Figure 4. Comparison of the potential for vibration suppression R for different values of κ (parameters: $\mu=0$, $B/D=0.5$)

to the bearing stiffness, the damping properties of the bearings can not entirely reach the disc, what narrows the effect. For $\kappa \rightarrow \infty$ the system behaves like a Jeffcott rotor in rigid bearings (concerning the resonance behavior), an influencing by the bearings is not possible.

3.2 Change of the Onset Speed of Instability

For a safe operation of a rotor system, the operational rotating speed should have a certain margin to the onset speed of instability. Above this speed, self-excited vibrations will occur, which lead to a damage or in the worst case to a destruction of a machine. Multi-lobe bearings are known for its good stability behavior in comparison to cylindrical bearings (comparison at $S_{O_{min}} = F_{stat} \psi_{min} / (B D \eta_{oil} \Omega) = \text{const.}$), see also the book of [Gasch et al. \(2001\)](#).

Figure 5 shows the onset speeds of instability for the same system parameters already used in figure 4. Generally, the onset speed of instability decreases with a decreasing shaft stiffness k . Furthermore it can be said, that the higher the specific Sommerfeld number is, the higher is the onset speed of instability (except for very small values of S_{O_0}). Comparing the graphs based on different preload factors, it turns out that for a decreasing shaft stiffness k (increasing κ) the individual onset speeds of instability are getting closer to each other. This is especially the case for low specific Sommerfeld numbers. For example for $\kappa=2$, here the difference nearly vanishes, the onset speed of instability depends mainly on ω_k .

As a conclusion, the application area for an adjustable journal bearing concerning the onset speed of instability is given for tendentially high specific Sommerfeld numbers and small values of κ .

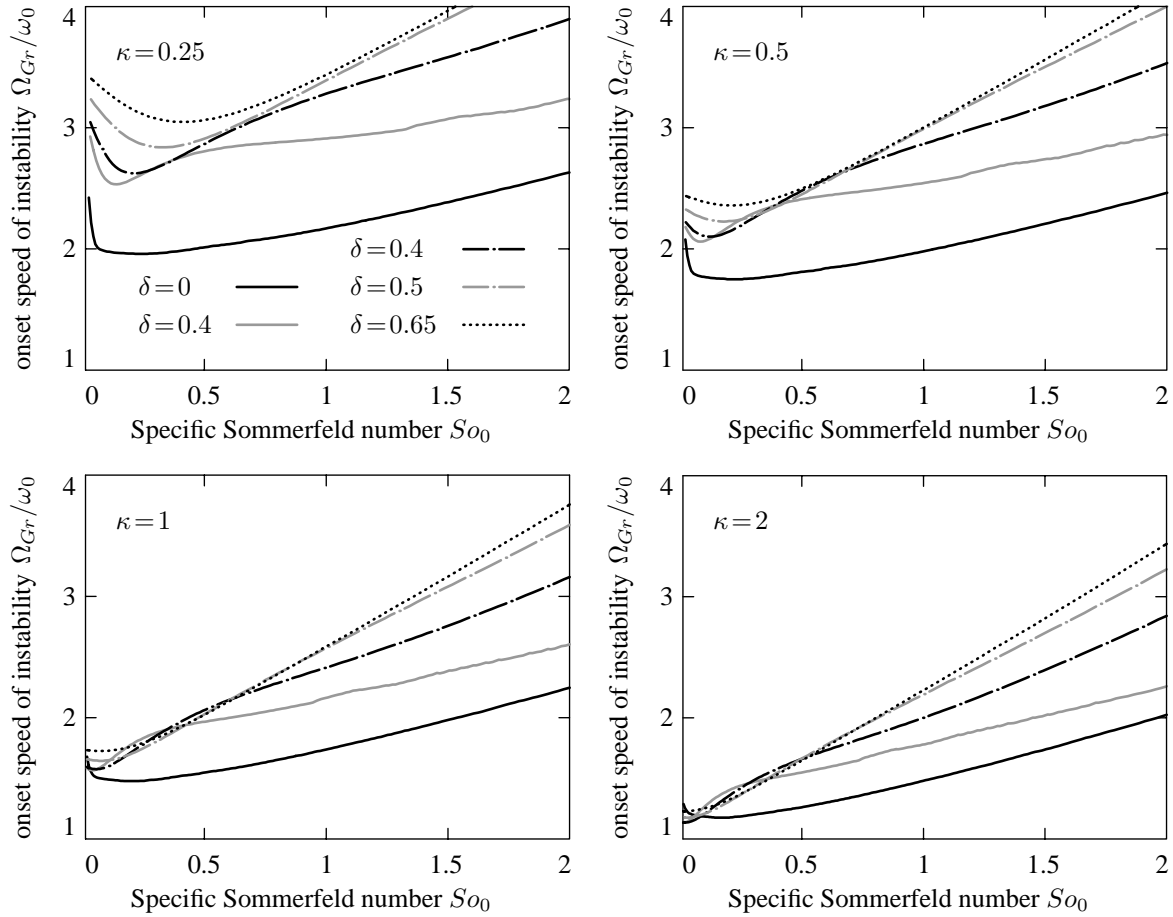


Figure 5. Comparison of the onset speeds of instability Ω_{Gr}/ω_0 for different values of κ (parameters: $\mu=0$, $B/D=0.5$)

3.3 Load carrying Capacity

A further subject is the load carrying capacity of the bearing. For this, the residual gap related to the minimal gap,

$$\frac{h_{res}}{h_{min}} = \frac{h_{res}}{h_n} \frac{1}{1-\delta}, \quad (7)$$

can be used as a measure, see also the book from [Lang and Steinhilper \(1978\)](#).

The higher the residual gap h_{res}/h_{min} , the higher is the load carrying capacity. A comparison of different bearing types (comparison at $S_{o_{min}} = F_{stat} \psi_{min} / (B D \eta_{oil} \Omega) = \text{const.}$) yields, that the cylindrical bearing has the highest load carrying capacity (see also [Lang and Steinhilper \(1978\)](#)). In the presented bearing design, the geometric shape and the minimal gap is changed due to the adjustment, at what the latter one has a higher influence.

Figure 6 shows the load carrying capacity for different preload factors. Mind that the curves are plotted against the Sommerfeld number S_o , due to the fact, that the load carrying capacity is a pure bearing property. For $\delta=0$, or in other words for the largest gap, the load carrying capacity is relatively low. Increasing the preload factor, respectively decrease the minimal gap, leads to a significant higher pressure build-up in the bearing and thus to a higher load carrying capacity. This effect is for lower Sommerfeld numbers more distinct. Note, that the load carrying capacity has to be reduced during the resonance pass trough.

It is to mention, that the non-referenced residual gap h_{min} is decreasing with an increasing preload factor δ for $S_o < 1$, for $S_o > 1$ it is nearly independent from δ .

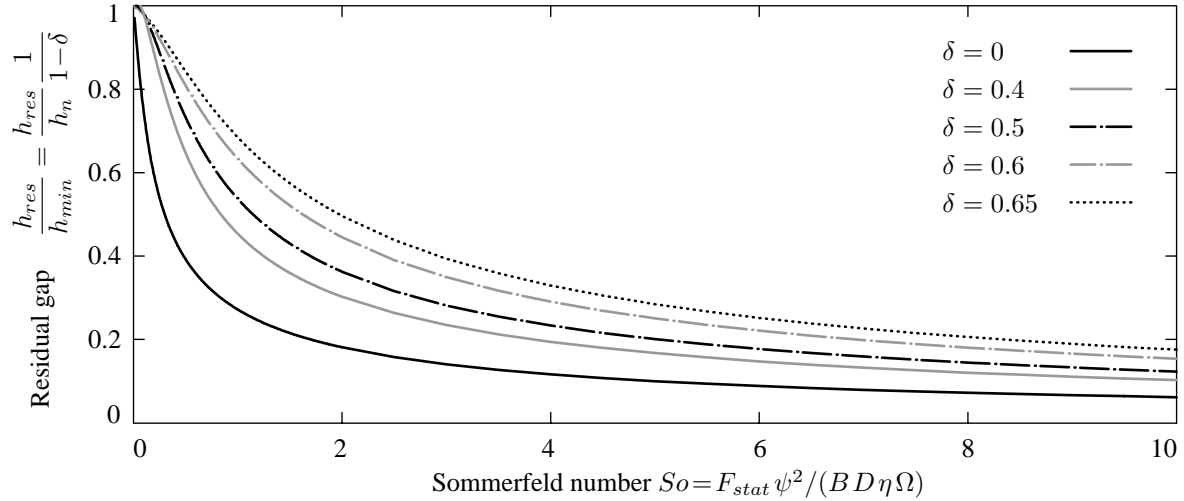


Figure 6. Residual lubrication gap in dependence of the Sommerfeld number for different preload factors

3.4 Conclusion

The investigation of a simple flexible rotor in adjustable journal bearings showed the fundamental effects concerning amplitude reduction, onset speeds of instability and load carrying capacity. If an application is useful in a real machine, these (and surely more) subjects have to be investigated for a specific machine design. As a simple rule it can be said, that the stiffness of the bearing and the shaft should be of the same order, respectively $\kappa = \mathcal{O}(1)$.

4 Experimental Setup and Validation

To validate the effect of amplitude reduction during the resonance pass trough, a test rig is set up, see figure 7. An AC-servomotor is used as drive, it is connected with a double cardan joint to the shaft. The shaft is supported by two ball bearings at the driving end, which function as simple suspension, and the adjustable journal bearing at the opposite side. The position of the upper bearing segment is adjusted by a high voltage piezo stack actuator with a maximum stroke of 200 μm . By means of an active magnetic bearing, additional stiffness and damping properties can be generated. In this manner, a change of the shaft stiffness and the influence of other damping sources can be investigated. Furthermore, the test rig contains two discs including retainer bearings.

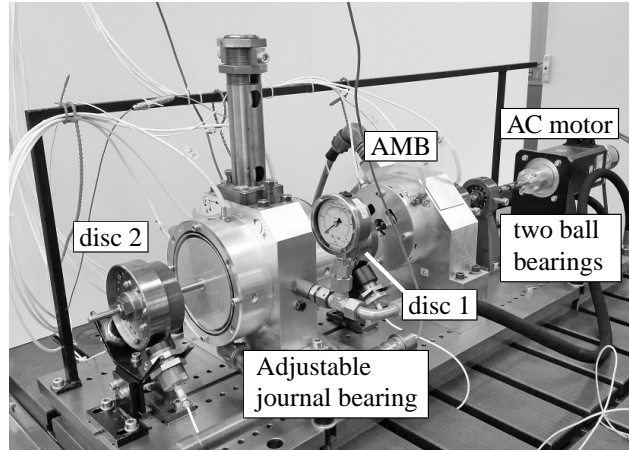


Figure 7. Picture of the test rig

Disc 1 is located between the magnetic bearing and the journal bearing, disc 2 is overhanging at the end of the test rig. Their deflections are measured using eddy current sensors. Due to its overhanging position, disc 2 shows the largest deflections, therefore it is mainly used for the analysis of the measurements.

The systems behavior is described by a MDOF model, see figure 8, using a modular system based on a finite element formulation. The shaft is modeled as Euler–Bernoulli beam, each individual element has a constant bending stiffness EI_j and a column mass density ρA_j . The journals of the magnetic bearing and the journal bearing are approximated as point masses, for the discs the moments of inertia are additionally considered. The forces from magnetic and journal bearing are indicated as F_{AMB} and F_L .

To update the model, a hammer testing of the running rotor (at $\delta = 0$) was performed. In a first step, masses and E -moduli were optimized to fit the first two bend-critical frequencies. After this, the damping was optimized using Rayleigh damping (stiffness term only), $\mathbf{B} = \beta \mathbf{K}$. The first bend-critical speed is about 1020 min^{-1} .

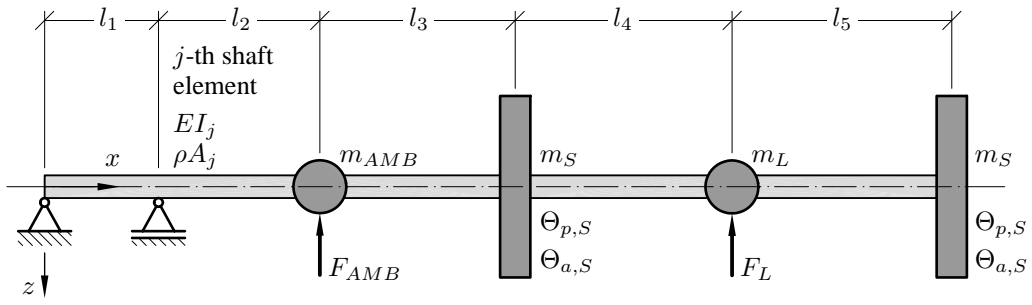


Figure 8. Mechanical model of the test rig

4.1 Run-up Processes

Figure 9 shows the measured and simulated results of two exemplary run-up processes. Here, the deflection of disc 2

$$|r_{S,2}| = \sqrt{w_{S,2}^2 + v_{S,2}^2}, \quad (8)$$

whose steady component is eliminated, is plotted against the time. The bearing forces were calculated with a non-linear force model (equation 3). Both, experiment and simulation exhibit that the maximum amplitude is increasing with the preload factor δ , as predicted in subchapter 3.1. The amplitude reduction for this example is about 24.2%. The agreement between experiment and simulation is satisfying.

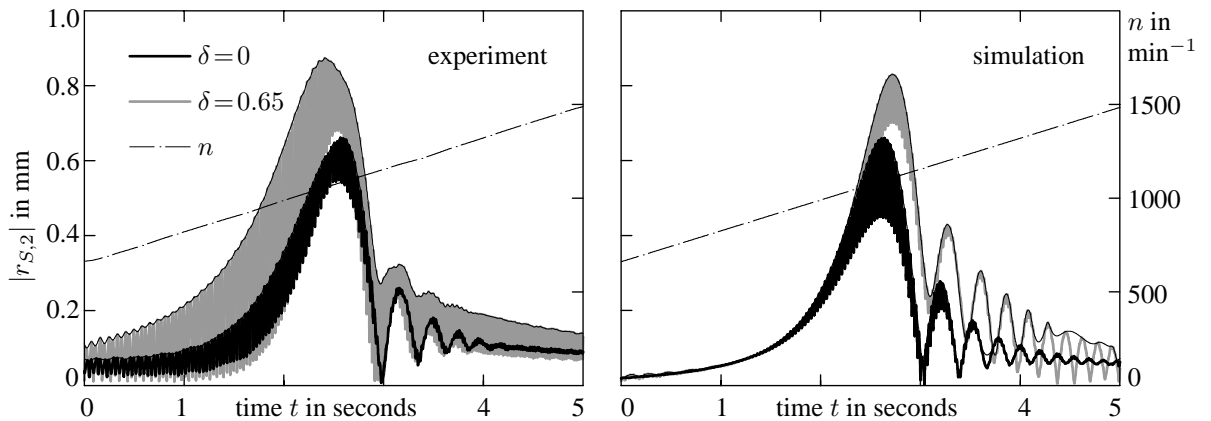


Figure 9. Exemplary run-up processes with different preload factors δ ; experiment (left) and simulation (right)

Run-up processes were carried out for different preload factors δ . Figure 10 shows the resulting maximum amplitudes in a bar graph. For low preload factors $\delta = 0 \dots 0.4$, the maximum amplitude is de facto the same. This is also predicted by the model (see also figure 2). A further increase of δ leads to higher maximum amplitudes. The reduction between $\delta = 0.7$ and $\delta = 0$ amounts to 25.2% and between $\delta = 0.7$ and $\delta = 0.3$ it is about 23.5%. Hence, the adjustment must not be accomplished over the full range of δ . For an application, the travel range of an actuator can be chosen smaller. Furthermore, the decrease of the load carrying capacity is not that large during the adjustment. The agreement between experimental and simulated results is satisfactory. The maximum deviation (at $\delta = 0.7$) is about 5%. A good result, considering that the model has been optimized for the value of $\delta = 0$. An optimization of the bearing model itself was not performed.

After the passage of the bending critical speed, the preload factor δ is set to larger value. A change of the stiffness and damping properties during the operation leads to natural vibrations. These vibrations decay quickly, due to the fact, that the damping ratios even after the resonance are relatively high. In general, the lower the change rate of the preload factor δ , the lower the arising natural vibrations.

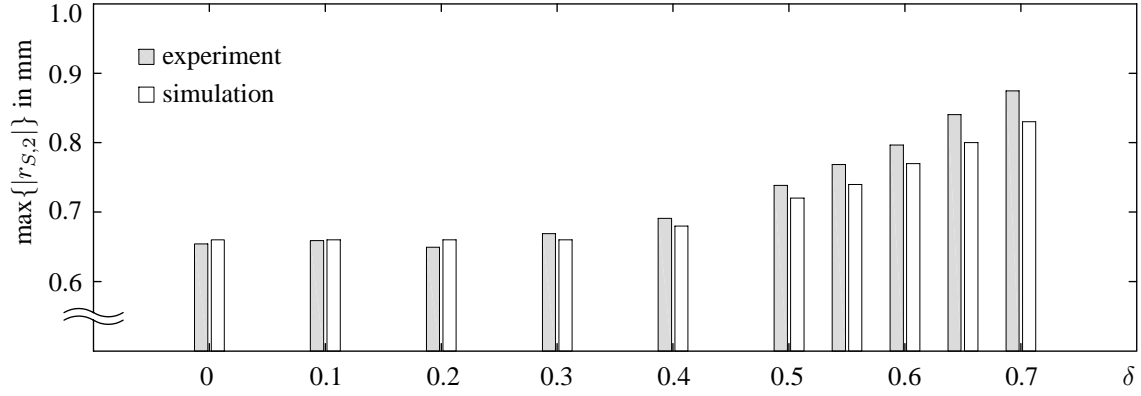


Figure 10. Comparison between measured and simulated resonance amplitudes for different preload factors δ

4.1.1 Additional stiffness and damping due to an active magnet bearing

To investigate the influence of a modified stiffness relation between shaft and bearing and to examine the influence of other damping sources in the system, experiments using the magnetic bearing were performed. The force of a magnetic bearing, here exemplary for the z -direction, operating with a PD controller is calculated and linearized to

$$F_{AMB} = (k_i P - k_s) w_1 + k_i D \dot{w}_1 = k_{AMB} w_1 + b_{AMB} \dot{w}_1. \quad (9)$$

At this, the parameters k_i and k_s are physical constants, P and D describe proportional and derivative gains. An operation with a pure P or D controller is not possible due to technical reasons, so both quantities have at all times values greater than zero.

For an adjustment of the stiffness relation, the proportional gain P is varied. The bend-critical frequency increases about 2.5 Hz, this corresponds to a decrease of κ . According to the theory, see figure 4, the amplitude reduction increases. Table 1 lists the result. A difference is detectable, but it is relatively weak. The standard deviation, calculated on a base of four measurements for each experiment, is one order smaller. However, the difference in amplitude reduction between minimal and maximal P -gain mounts to 3.8 percentage points.

Table 1. Maximum amplitudes $\max\{|r_{S,2}|\}$ in dependence of different proportional gains P ($D=0.01$ As/mm)

proportional gain	$\delta=0$	$\delta=0.65$	Reduction
$P=10$ A/mm	0.790 mm	1.045 mm	24.3%
$P=15$ A/mm	0.762 mm	1.041 mm	26.8%
$P=20$ A/mm	0.743 mm	1.034 mm	28.1%

In a real-world rotor, there are several sources of damping, for example due to a surrounding fluid, material damping or other bearings. To capture this influence, experiments with different derivative gains D have been carried out. The results are listed in table 2. At these experiments, the difference between minimal and maximal D gain is about 7 percentage points. Hence, additional damping can decrease the effect of amplitude reduction. For an eventual designing of a rotor system with an adjustable journal bearing, potential damping sources should be considered.

Table 2. Maximum amplitudes $\max\{|r_{S,2}|\}$ in dependence of different derivative gains D ($P=10$ A/mm)

derivative gain	$\delta=0$	$\delta=0.65$	Reduction
$D=0.01$ As/mm	0.795 mm	1.078 mm	26.3%
$D=0.03$ As/mm	0.622 mm	0.788 mm	21.1%
$D=0.05$ As/mm	0.551 mm	0.682 mm	19.3%

4.2 Measured and calculated Onset Speeds of Instability

Besides the run-up simulations, also the onset speeds of instability were measured. For this purpose the rotational speed is raised in small steps. If the rotor starts to carry out vibrations with the bend-critical frequency, what is good to observe in a real-time FFT, the onset speed of instability is found and the rotational speed has to be lowered immediately to avoid damage. This procedure is repeated for several values of the preload factor δ .

Figure 11 shows the experimental and numerical results. The present behavior – a decrease of the onset speed of instability for high preload factors – is not observed in this extent investigating the Jeffcott rotor. The reasons for this are effects, which are not shown by the investigated Jeffcott rotor, this is for example a shift of the onset speed of instability caused by gyroscopic effects due to the overhung disc. An important point is, that experiment and simulation show a similar global behavior. However, the differences between measured and simulated results are with values up to 15% satisfying only to a limited extent. Even comparing theoretical results based on different bearing data results in a relatively high scattering.

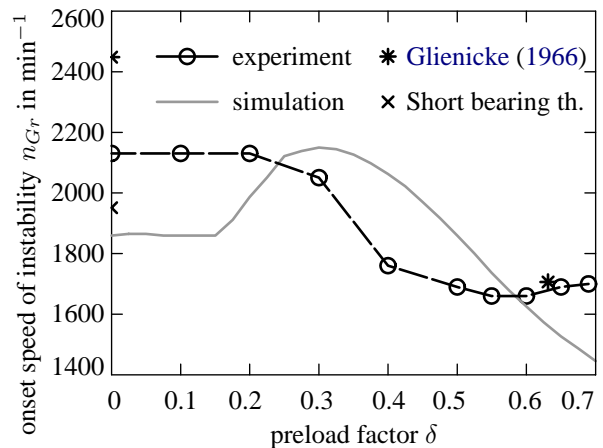


Figure 11. Measured and calculated (based on bearing data from different sources) onset speeds of instability

The determination of onset speeds of instability is especially for non-circular bearings difficult, due to the fact that a small change in the Sommerfeld number (e. g. by a change of the oil temperature) can lead to a significant change of the results (see also Gasch et al. (2001)).

5 Conclusions

In this paper, an adjustable journal bearing for the vibration reduction of flexible rotors is presented. An investigation of the Jeffcott rotor supported by such bearings shows the basic effects. It turns out, that a designing has to be made among others with respect to the reduction of the maximum amplitude during the resonance pass trough, the onset speed of instability and the load carrying capacity. For a validation, a test rig is set up. The experimental results show, that the effect of amplitude reduction arises. Numerical results using a simple mechanical model agree with the experiments. Furthermore, the influence of additional stiffness and damping properties is investigated, which influence the maximum amplitude more or less. Finally, measured and calculated onset speeds of instability were compared.

References

- Althaus, J.: *Eine aktive hydraulische Lagerung für Rotorsysteme*. Fortschritt-Berichte VDI Reihe 11 Nr. 154, VDI-Verlag, Technische Universität München (1991).
- Becker, K.; Seemann, W.: A journal bearing with actively modified geometry for extending the parameter-based stability range of rotor dynamic systems. In: *Euromech Colloquium 573 - Coupling and Nonlinear interactions in Rotating Machinery* (2015).
- Breunung, T.; Dohnal, F.; Pfau, B.: An approach to account for multiple interfering parametric resonances and anti-resonances applied to examples from rotor dynamics. In: *Proceedings of the 12th International Conference on Vibrations in Rotating Machines (SIRM)*, Graz, Austria (February 2017).
- Chasalevris, A.; Dohnal, F.: A journal bearing with variable geometry for the reduction of the maximum amplitude during passage through resonance. *Journal of Vibration and Acoustics*, 134, (2012), 061005–1–061005–8.
- Chasalevris, A.; Dohnal, F.: Vibration quenching in a large scale rotor-bearing system using journal bearings with variable geometry. *Journal of Sound and Vibration*, 333, (2014), 2087–2099.

- Chasalevris, A.; Dohnal, F.: A journal bearing with variable geometry for the suppression of vibrations in rotating shafts: Simulation, design, construction and experiment. *Mechanical Systems and Signal Processing*, 52-53, (2015), 506–528.
- DIN: DIN-Norm 31657-1 Hydrodynamische Radial-Gleitlager im stationären Betrieb, Teil 1: Berechnung von Mehrflächen- und Kippsegmentlagern (1996).
- Dohnal, F.; Pfau, B.; Chasalevris, A.: Analytical predictions of a flexible rotor in journal bearings with adjustable geometry to suppress bearing induced instabilities. In: *Proceedings of the 13th International Conference on Dynamical Systems - Theory and Applications*, Łódź, Poland (December 2015).
- El-Shafei, A.; Dimitri, A. S.: Controlling journal bearing instability using active magnetic bearings. *Journal of Engineering for Gas Turbines and Power*, 132(1), (2010), 012502–012502–9.
- Fürst, S.; Ulbrich, H.: An active support system for rotors with oil-film bearings. In: *Proceedings of the 4th International Conference on Vibrations in Rotating Machinery of the Institution of Mechanical Engineers*, pages 61–68, Edinburgh, UK (1988).
- Gasch, R.; Nordmann, R.; Pfützner, H.: *Rotordynamik*. Springer-Verlag (2001).
- Glienicke, J.: *Feder- und Dämpfungskonstanten von Gleitlagern für Turbomaschinen und deren Einfluß auf das Schwingungsverhalten eines einfachen Rotors*. Ph.D. thesis, Technische Hochschule Karlsruhe (1966).
- Köhl, W.: *Stabilisierung von leichten Rotoren in Schwimmbuchsenlagern durch statisch unbestimmte Lagerung*. Ph.D. thesis, Technische Universität Darmstadt (2015).
- Krodkiewski, J. M.; Cen, Y.; Sun, L.: Improvement of stability of rotor system by introducing a hydraulic damper into an active journal bearing. *International Journal of Rotating Machinery*, 3, 1, (1997), 45–52.
- Lang, O.; Steinhilper, W.: *Gleitlager – Berechnung und Konstruktion von Gleitlagern mit konstanter und zeitlich veränderlicher Belastung (Konstruktionsbücher Band 31)*. Springer-Verlag (1978).
- Martin, J. K.; Parkins, D. W.: Theoretical studies of a continuously adjustable hydrodynamic fluid film bearing. *Journal of Tribology*, 124, (2002), 203–211.
- Pfau, B.: *Numerische Untersuchung eines Rotors in Schwimmbuchsenlagern*. Masterthesis, Technische Universität Darmstadt (2012).
- Pfau, B.; Markert, R.: Konstruktion und Erprobung eines Zweiflächengeitlagers mit verstellbarer Spaltgeometrie zur Reduzierung der Schwingungen von flexiblen Rotoren. In: *Second IFToMM D-A-CH Conference 2016*, Innsbruck, Austria (February 2016).
- Pfau, B.; Rieken, M.; Markert, R.: Numerische Untersuchungen eines verstellbaren Gleitlagers zur Unterdrückung von Instabilitäten mittels Parameter-Antiresonanzen. In: *First IFToMM D-A-CH Conference*, Dortmund, Germany (March 2015).
- Przybyłowicz, P.: Active stabilisation of a rigid rotor by a piezoelectrically controlled mobile journal bearing system. *Australian Journal of Mechanical Engineering*, 1(2), (2004), 123–128.
- Santos, I. F.: On the future of controllable fluid film bearings. *Mécanique & Industries*, 12, (2011), 275–281.
- Santos, I. F.; Scalabrin, A.: Control system design for active lubrication with theoretical and experimental examples. *Journal of Engineering for Gas Turbines and Power*, 125, (2003), 75–80.
- Someya, T.: *Journal-Bearing Databook*. Springer-Verlag (1989).
- Tůma, J.; Šimek, J.; Škuta, J.; Los, J.: Active vibrations control of journal bearings with the use of piezoactuators. *Mechanical Systems and Signal Processing*, 36, (2013), 618–629.
- Ulbrich, H.; Althaus, J.: Actuator design for rotor control. In: *12th Biennial ASME Conference on Vibration and Noise*, pages 17–22, Montreal, Quebec, Canada (September 1989).
- Wu, A.; de Queiroz, M.: A new active tilting-pad bearing: Nonlinear modeling and feedback control. *Tribology Transactions*, 53, 5, (2010), 755–763.